Genetically magnetic control of neural system *via* TRPV4 activation with magnetic nanoparticles

Songfang Wu [a,1], Hong Li [a,1], Dongqi Wang [b], Luming Zhao [a], Xin Qiao [a], Xiao Zhang [a], Wei Liu [a], Changyong Wang [a,*], Jin Zhou [a,*]

[a] *Beijing Institute of Basic Medical Sciences, 27 Taiping Rd, Beijing 100850, PR China*
[b] *Multidisciplinary Initiative Center, Institute of High Energy Physics, Chinese Academy of Sciences, Beijing 100049, PR China*

ARTICLE INFO

ABSTRACT

In recent years, various kinds of nanomaterials based invasive or non-invasive deep neural stimulation tools are developed for modulating neural system and illuminating the relationship between neural circuits and specific behaviors. For better modulation of neural system and clinical application, the neural stimulation nanotools should be optimized. In this work, we demonstrated a novel non-invasive neural modulation approach relying on magnetic field, which is realized by modifying magnetic nanoparticles (MNPs) with anti-His antibody and inserting His-tag at specific position of TRPV4 to target the activation of TRPV4 ion channel. The activated TRPV4 ion channel could induce the calcium influx by *in vitro* calcium imaging assay in cultured neurons. This study showed that this approach can improve the calcium transient compared with unmodified MNPs. Furthermore, this approach was confirmed in freely moving mice presenting valid magnetic control of rotation around the body-axis and freezing of gait. This work demonstrates that TRPV4 ion channel can be activated by MNPs based nanotool, which provides a new alternative way for achieving magnetic stimulation in deep-brain circuits. This work also can serve as a useful validation study for magnetogenetics.

Introduction

Understanding how the brain dictates the behavior of animals is the HollyGrail in the study of system neuroscience. Artificial regulation and intervention by deep stimulation of the neural system is the main means to study the function of various brain regions and the correlation between brain regions, and to regulate the specific nerve cell types accurately. In order to realize precise inhibition and excitation of neural network, offer insight into the functional significance of neural system activity and enrich our understanding of the relationship between neural system and specific animal behaviors, in recent years, effective neural stimulation tools based on various kinds of nanomaterials such as nanoparticles, nanowires and nanotubes are developed [1–3]. This is because the small sizes and high surface-to-volume ratios of nanomaterials make them have enhanced and exceedingly good physical properties and show unique opportunities in biology [4–7].

The nanomaterials based neural stimulation tools can be divided into several types according to different stimulation modes, for instance, carbon nanotube based miroelectrodes for deep brain electric stimulation [8,9], various types of nanoparticles for optogenetic stimulation [10,11], piezoelectric nanoparticles/nanotubes for ultrasounds stimulation [12,13] and magnetic nanoparticles for magnetic stimulation [14], *etc.* Among these nanotools, the optical genetic nanotools with the advantage of high spatial, temporal, and neurochemical resolution have been widely used in the regulation of rodent behavior, and are helpful for understanding of the specific functions of various specific neural pathways related to behavior [15]. However, due to the scarce penetration of the light through the tissues, most optogenetic stimulation methods needs implantation of optical waveguides, which, like the implanted miroelectrodes for deep brain electric stimulation, can result in the inflammation and

---

gliosis at the implant site [13]. Therefore, it is necessary to develop other nanotools for non-invasive clinical stimulation treatments.

Compare with optogenetic stimulation methods, magnetic fields can penetrate deeper into the brain, which offers an alternative non-invasive way. It enables magnetic nanoparticles based magnetic stimulation has the characteristics of deep and targeted stimulation of specific brain regions and remote regulation of neural circuits related to animal behavior [14]. Published studies on magnetic stimulation of neural circuits mainly induced calcium influx of cells by activating transient receptor potential vanilloid 1 or 4 (TRPV1 or TRPV4), which are vital ion channels and mainly sensitive to magnetic nanoparticles induced magnetothermal heating (42 °C) and mechanical force, respectively [16–22]. In 2015, *Chen* et al. reported that under the action of interactive magnetic field, the magnetic nanoparticles (MNPs) can dissipate heat, cause the reversible discharge of TRPV1+ nerve cells in the surrounding, and then generate biological stimulation in the target area of brain [16]. The injection of magnetic nanoparticles maintained its impact on the brain for one month, creating chronic stimulation without implantation. The magnetic nanoparticles used in this experiment were not specifically modified, and displayed high off-target behavior, thus could not accurately target cells, a larger amount of MNPs and heat consumption are demanded to activate more cells. However, overheating is a harmful general effect related to heat dissipation in brain. By inserting a His tag into the TRPV channel and encasing magnetic nanoparticles with anti-His antibodies, this magnetothermal stimulation method can be optimized [19,20].

For the work related to magnetic stimulation by activating TRPV4 (*i.e.* mechanosensitive channels), in 2016, *Wheeler* et al. synthesized a single component, magnetically sensitive actuator, "Magneto," through fusion of the non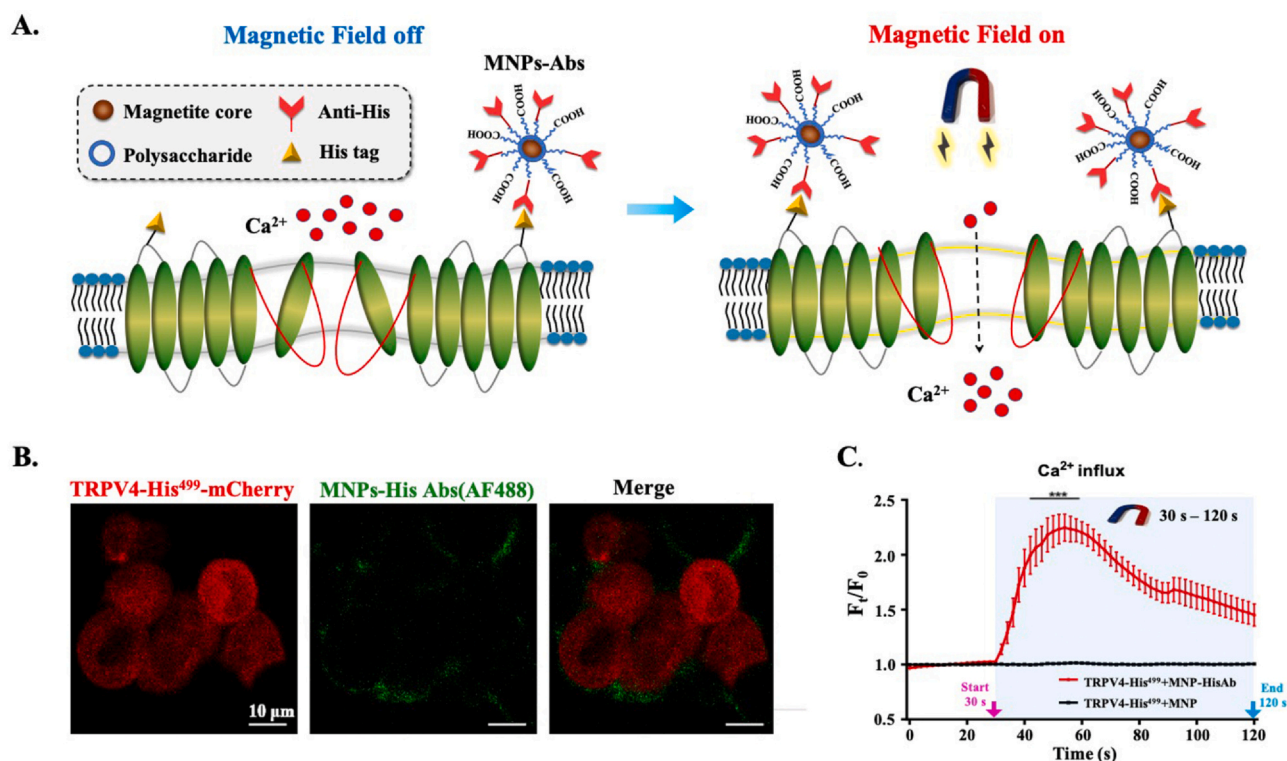-selective cation channel, TRPV4, to the paramagnetic protein, ferritin, which requires only one injection and its using has been validated both *in vitro* and *in vivo* [18]. MNPs have been proven to be an effective nanotool to activate TRPV1, however, whether they can be used to activate TRPV4 is still unreported.

In this work, we fabricated a magnetic field-driven nanotool through inserting His-tag at specific position of TRPV4 and using anti-His antibody modified MNPs, and have successfully applied it to stimulate neural system. Calcium imaging assay in HEK293T cells and cultured neurons *in vitro* demonstrated effective activation of calcium transient, suggesting the TRPV4 ion channel could be activated by MNPs under the stimulation of magnetic field. The observation that specific mice behaviors change during magnetic field stimulation indicated that TRPV4-MNPs engagement successfully triggered the activation of two separate brain regions, dorsal striatum and the ridge between dorsal and ventral striatum. Although two injections are needed in this method of TRPV4-MNPs, MNPs exhibits sensitive to magnetic field and negative effects including off-target and overheating can be reduced, demonstrating this work offers a new method for realizing magnetic stimulation by activating TRPV4. Additionally, magnetogenetics has not been widely adopted due to the concerns about its ease of use [23] and validity [24], as a consequence, this work also provides a useful validation study for magnetogenetics.

Results

Principles of magnetic force driven neural stimulation

Based on the researches of TRPV4 and MNPs, we designed a magnetic sensitive nanotool *via* the insertion of His tag into TRPV4 attached to MNPs (Fig. 1A). 6×His tag was inserted into the

Fig. 1. Cell membrane-bound MNPs modulates the calcium influx in HEK293T cells. A. MNPs decorated with anti-His tag antibody binds to the His tag of TRPV4 ion channel, and elicits calcium influx during the magnetic stimulation. B. Laser confocal image of TRPV4-His499-mCherry overexpressed HEK293T cells (red). AF488-anti-His antibody modified MNPs (green) bound to the cell membrane. Scale bar is 10 μm long. C. *In vitro* Calcium imaging fluorescence fold change in response to 50 mT magnetic stimulation (0.1 Hz, 90% duty cycle, the period of electric magnet stimulation is 30–120 s). Only in TRPV4-His499 overexpressed cells (Fluo-4AM loaded) together with His Abs modified MNPs (red line) could elicit calcium influx during magnetic field stimulation. Fluorescence fold change of n > 10 cells of three independent experiments were analyzed for each condition. (Two-way ANOVA, p < 0.0001).

extracellular loop of TRPV4 through molecular cloning, and the fusion protein was expressed by plasmid transfection or virus transduction in different cell types. Anti-His antibody modified MNPs were added to cell culture medium, and bound to TRPV4 protein on the cell surface. Under the stimulation of magnetic field, MNPs activated TRPV4 ion channel, triggered the calcium influx in cells, and interfered the calcium related function of cells.

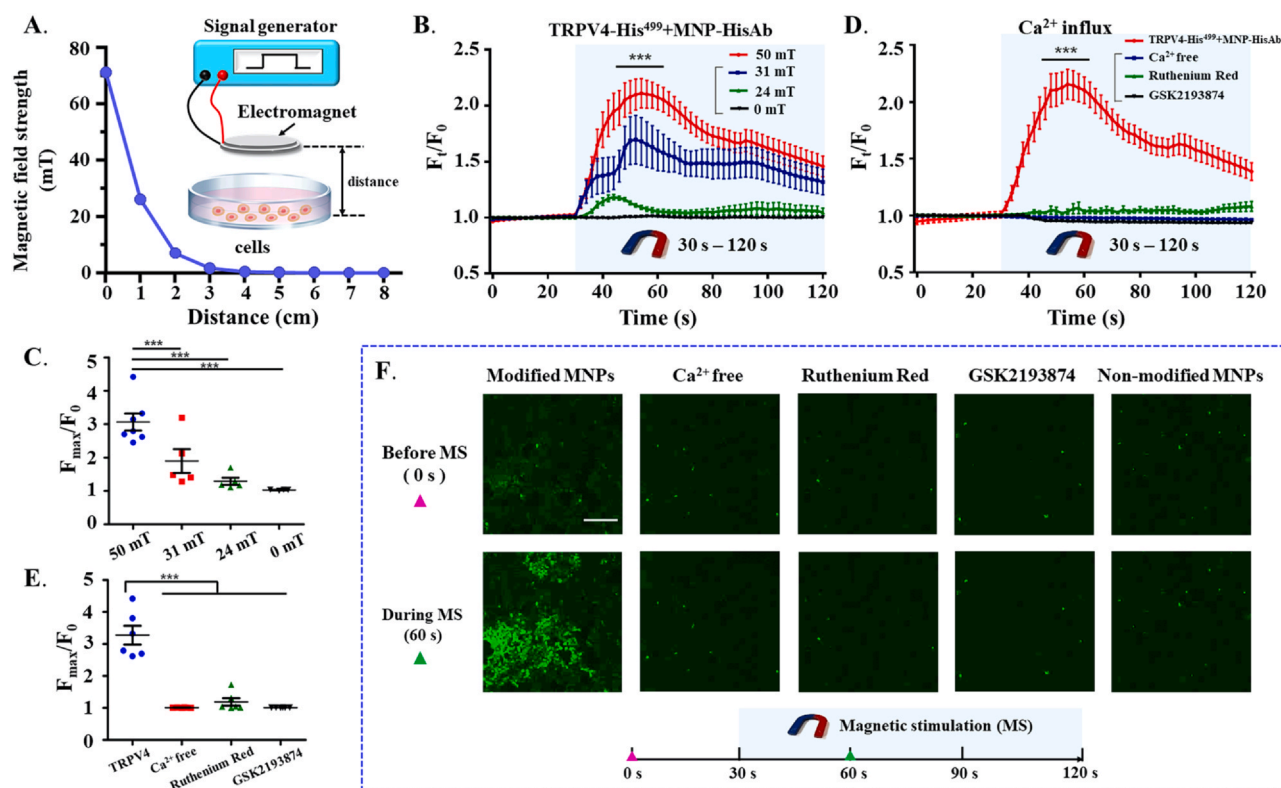*Development of an optimal magnetic sensitive nanotool*

Commercial superparamagnetic magnetic nanoparticles functionalized with carboxyl group (Cat: fluidMAG 4115–100 nm, Chemicell) were used for the activation of TRPV4 in our design. This ferrofluids can be used for MRI-diagnostics and magnetic drug targeting applications [25–27]. FluidMAG-nanoparticles with hydrodynamic diameters of 100 nm have a multi-domain core (Information provided by Chemicell) which means they always form small clusters about 100 nm when used in assay (Fig. S1A). The magnetite cores of MNPs were shown in transmission electron micrographs with an average size of 19 ± 8 nm (Table S1).

Anti-His antibody or Anti-His antibody-AF488 (Santa Cruz) was used for the modification of MNPs (Fig. S2). Catalyzed by NHS, carboxyl groups of MNPs formed covalent bond with amino groups of the antibodies. Additionally, MNPs and Abs-modified MNPs showed perfect dispersibility in water (Fig. S3), which is necessary for the brain stereotactic injection of MNPs. The magnetite cores and shells of MNPs and Abs-modified MNPs were shown in transmission electron micrographs (Fig. S1B). Abs modification efficiency was determined by measuring non-coated antibody concentration by micro BCA assay (Table S1).

In order to achieve the objectives of concept in Fig. 1A, we did the *in vitro* calcium imaging assay in HEK293T with the over-expression of TRPV4-His499 to test the performance of our designed magnetic sensitive nanotool. Details of calcium imaging assay were illustrated in Methods. The binding of Abs-MNPs and cells were detected by confocal imaging, as shown in Fig. 1B, Abs-MNPs (AF488) (green) located on the surface of TRPV4-His499-mcherry plasmid transfected HEK293T cells (red). About 70%–80% cells are transfected by TRPV4-His499-mCherry plasmid (Fig. S4). Cells overexpressing TRPV4-His499 exhibited significant enhancement of Fluo-4 fluorescence after being stimulated by a 50 mT magnetic field delivered by electric magnet (Fig. 1C). The 50 mT magnetic field was produced by placing the magnet ~0.5 cm above the cells (Fig. 2A). Cytotoxicity test of MNPs was performed by incubating HEK293T cells with or without 100 μg MNPs for 30 min, 1 day, 2 day and 3 day, respectively, though live/dead staining (Fig. S5A). Additionally, biocompatibility *in vitro* assessed by measuring the OD value of HEK293T incubated with different concentration of MNPs using Cell Counting Kit-8 assay (Fig. S5B). These results confirmed the good cell biocompatibility of MNPs.

Considering that TRPV4 is also a temperature sensitive channel like TRPV1, temperature about 42 °C could activate the channel. After the cells were just taken out from the cell incubator, the temperature variation of culture media during the calcium imaging assay was recorded before (0–30 s) and during loading the magnetic field (30–190 s). Obviously, there was no increase in temperature (Fig. S6).

Fig. 2. Magnetic field strength dependent control of calcium influx and TRPV4 is the dominant calcium channel during the stimulation process. A. Electric magnets deliver a distance dependent magnetic field. The inset shows the arbitrary waveform generator guided magnetic field generation system. B. Fluorescence fold (F_t/F_0) of calcium influx elicited by different magnetic field strengths in HEK293T cells transfected with TRPV4-His499 in the presence of MNPs-HisAb. N > 10 cells of three independent replicates were analyzed. (Two-way ANOVA, p < 0.0001) C. Calcium fluorescence fold change of randomly selected cells with n > 4 independent replicates under each condition, and 10 cells for each replicate. (One-way ANOVA, p < 0.0001) D. Average kinetics of Fluorescence fold change of TRPV4-His499-MNP-HisAb, Calcium free, ruthenium red (RR), and GSK2193874 groups, respectively. n > 30 cells of three independent replicates were analyzed. (Two-way ANOVA, p < 0.0001) E. Quantification of calcium fluorescence fold change for different conditions. Randomly selected cells of n > 5 independent replicates were analyzed for each condition, and 10 cells for each replicate. (One-way ANOVA, p < 0.0001) F. Calcium imaging micrographs of HEK293T cells before magnetic stimulation (MS) and during MS. Different conditions show the changes of Fluo-4 fluorescence. Scale bar is 200 μm long. Related Videos are available in supplementary data.
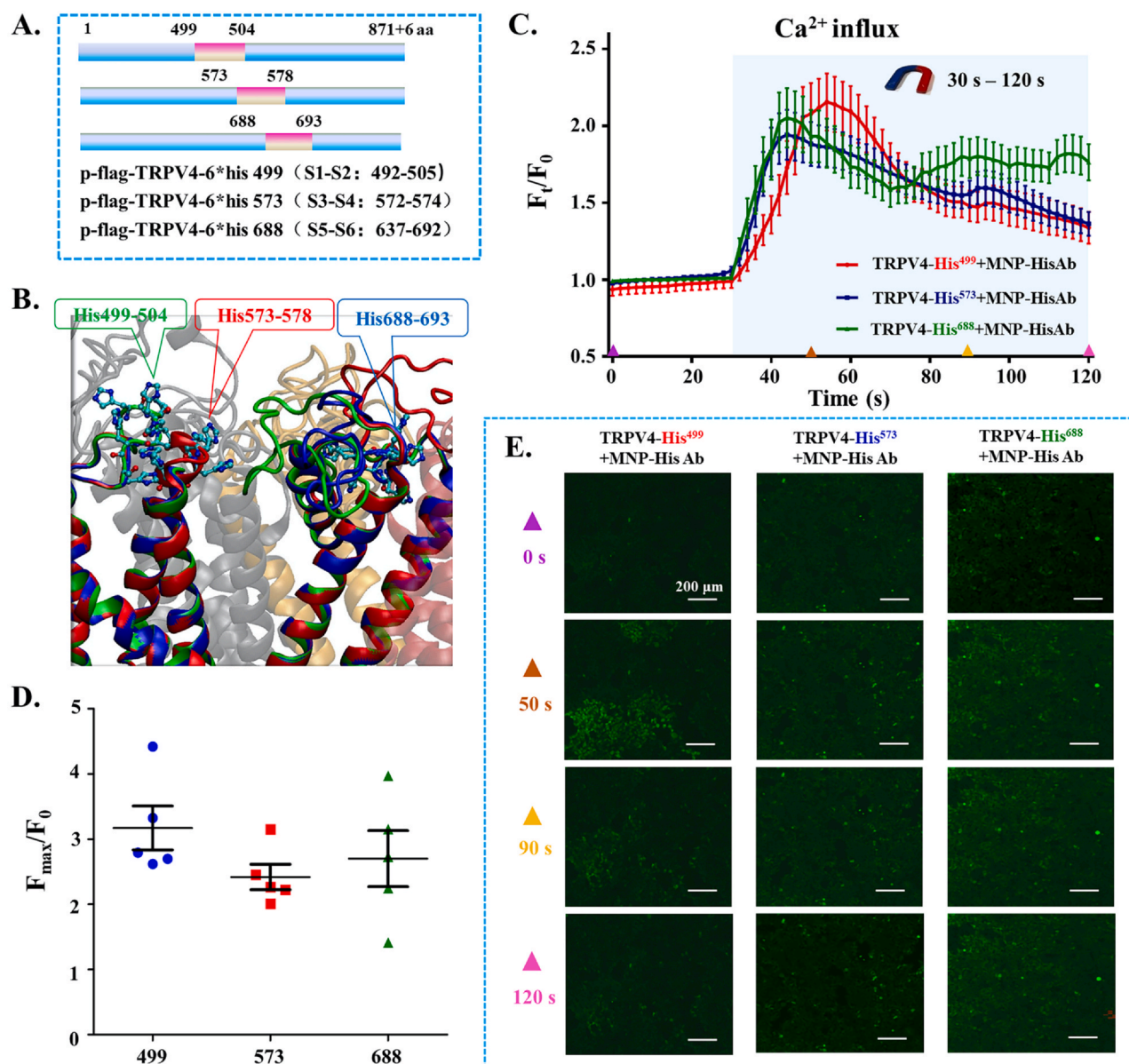
The temperature of the culture media was measured by temperature probe of magnetic stirrer in the laboratory with a temperature of 25 degrees.

The influence of magnetic field strengths on the activation of TRPV4 in HEK293T cells was investigated by using magnetic fields of about 50 mT, 31 mT, 24 mT and 0 mT, which was realized by varying the distance between the electromagnet and cells (Fig. 2A). Fluorescence fold changes of different magnetic field strengths elicited corresponding calcium influx in HEK293T cells transfected with TRPV4-His499 in the presence of MNPs-HisAb were shown in Fig. 2B. The fluorescence fold (F_t/F_0) of calcium influx showed dependence on magnetic field strength and higher magnetic field strength could elicit more dramatically increase of intracellular calcium (Fig. 2C). By using TRPV antagonist (ruthenium red), TRPV4 specific inhibitors (GSK2193874), and calcium free medium as control, respectively (Fig. 2D–F, Movie S1-S5), TRPV4 was identified to be the dominant calcium channel responsible for the magnetic field induced calcium transient, and our magnetic sensitive nanotool composed of TRPV4-His499 and Anti-His antibody MNPs were successfully verified in vitro.

Supplementary material related to this article can be found online at doi:10.1016/j.nantod.2021.101187.

Based on the analysis of the reported Cryo-EM structure of TRPV4 [28], we designed three different insertions of 6×His tag into the extracellular loops of TRPV4 (Fig. 3A), denoted as TRPV4-His499, TRPV4-His573, and TRPV4-His688, respectively. Molecular modeling of TRPV4 tetramer proteins showed that the inserted His tags located in the extracellular part of TRPV4 (Fig. 3B) and extended the length

Fig. 3. Calcium influx induced in 293 T cells by different His tag insert position of TRPV4. A. Three different TRPV4-His expression plasmids based on the Cryo-EM structure of TRPV4 protein. B. molecular modeling of three different insertions. C. Average kinetics of Fluorescence fold change of three different conditions. N > 30 cells of three independent replicates were analyzed. Over-expression of TRPV4-His499 (red), TRPV4-His573 (blue), or TRPV4-His688 (green) in HEK293T cell induces corresponding calcium transits. The data were analyzed by two-way ANOVA (no significance). D. Quantification of calcium fluorescence fold change under different conditions. Randomly selected cells of n > 5 independent replicas were analyzed under each condition, and 10 cells for each replicate. The data were analyzed by one-way ANOVA (no significance). E. Calcium imaging micrographs of HEK293T cells transfected with TRPV4-His499, TRPV4-His573 or TRPV4-His688 plasmids show the changes of fluo-4 fluorescence in time course. Scale bar is 200 μm long. Related videos are available in supplementary data.

of loops. The insertion of His tag did not affect native folds of TRPV4 and its secondary and tertiary structure of TRPV4 were conserved (Fig. S7). His tags in TRPV4-His[499] and TRPV4-His[688] did not change the conformation of the loops (S1-S2, S5-S6), while the His tag of TRPV4-His[573] became part of the loop (S3-S4). A superimposition of the structures of TRPV4 and TRPV4-His[499] was shown in Fig. S8.

The behavior of other two His-tagged TRPV4 (TRPV4-His[573], and TRPV4-His[688]) were also investigated through calcium imaging and compared with TRPV4-Hi[499]. Both TRPV4-His[573] and TRPV4-His[688] induced significant increase of intracellular calcium (Fig. 3C-E, Movies S6-S7), but less than by TRPV4-His[499], implicating the S1-S2 domain caused stronger response than the S3-S6 domain in the calcium transportation. Detailed mechanism responsible for the difference remains to be studied.

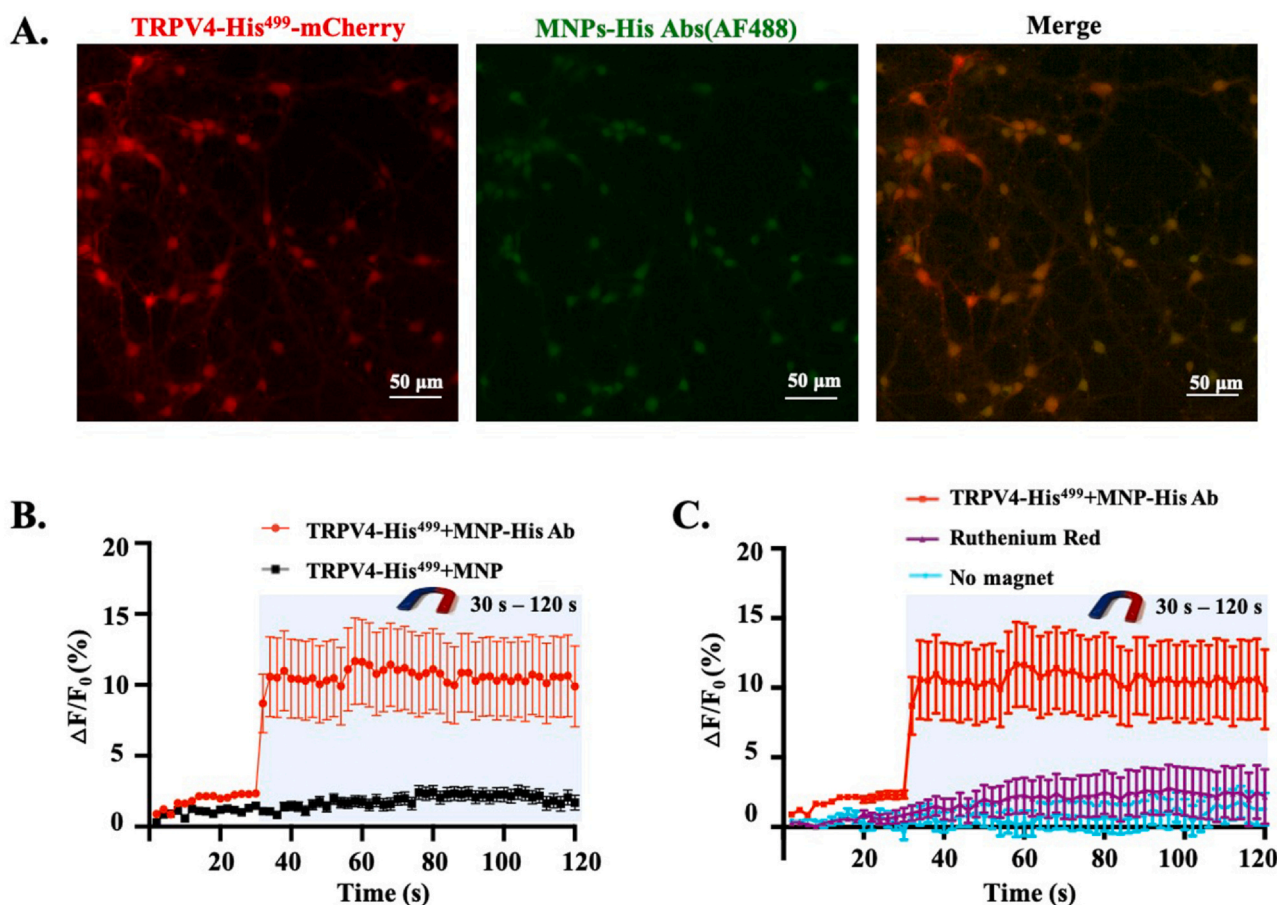Supplementary material related to this article can be found online at doi:10.1016/j.nantod.2021.101187.

Verification effectiveness of magnetic sensitive nanotool in neural activation

To apply the magnetic sensitive nanotool in neural system, we test its effectiveness in cultured cortical neurons. Mice cortical neurons were acquired and seeded on chamber slides. TRPV4-His[499] was expressed in cultured cortical neurons by adeno-associated viruses (AAV) transduction after 7 days' culture and TRPV4-His[499]-p2A-mCherry expression was presented (Fig. 4A). Abs-MNPs (AF488) (green) were located on the surface of TRPV4-His499-mcherry neuron (red) (Fig. S9). Magnetic field was placed above the chamber
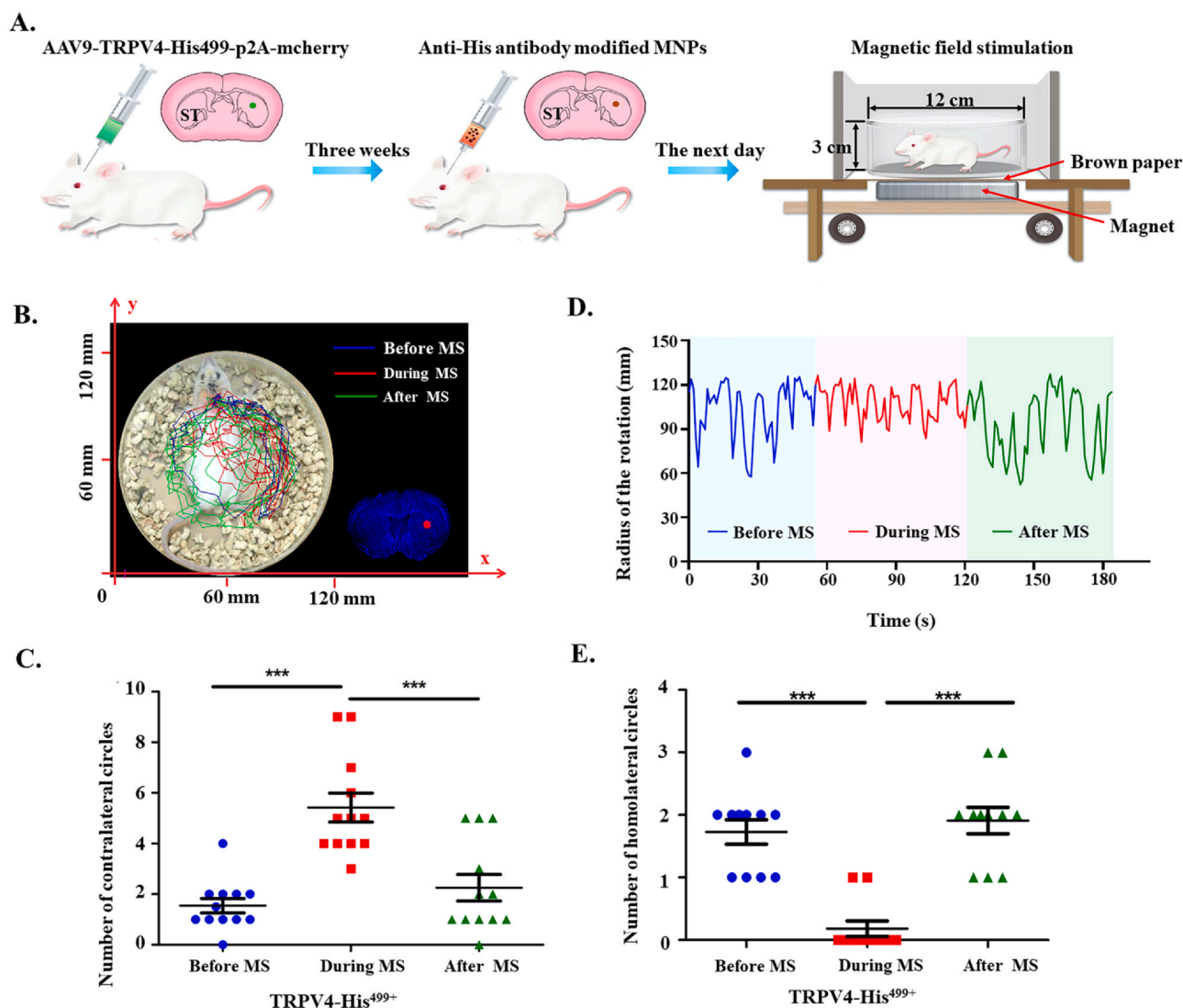
slides with a distance of less than 0.5 cm for the generation of about 50 mT magnetic field. Fluorescence micrographs of neurons transducted with TRPV4-mCherry shows significant Ca^{2+} influx through Ca^{2+} indicator (Fluo-4, AM) under magnetic stimulation (Fig. 4A), that suggested the magnetic sensitive nanotool could activate cultured cortical neurons and was useful to modulate neural activity. Calcium imaging fluorescence fold change of TRPV4-His499-MNP-HisAb was higher than TRPV4-His499-MNP in response to magnetic stimulation (Fig. 4B). By using ruthenium red (Fig. 4C), TRPV4 was identified to be the dominant calcium channel responsible for the magnetic field induced calcium transient in cultured cortical neurons.

Deep brain magnetic force drove stimulations in striatum cause rapid rotations around body axis

We next validated the use of TRPV4-His-MNPs in the control of animal behaviors *via* activation of targeted neurons. Reported assays confirmed that both chemogenetic and magnetothermal activation of the caudate putamen nuclei in striatum, a deep region of brain, could evoke increased locomotion in the form of unilaterally rotation around the body axis [29,30]. Based on the reported precise stereo-position of caudate putamen nuclei in striatum, 1 μL AAV2/9-hSYN-TRPV4-His499-P2A-mCherrry-WPREs (experimental group) and AAV2/9-hSYN-P2A-mcherry-WPREs (control group) were respectively injected into the mice brain at the speed of 100 nL/min by microsyringe (HAMILTON 65461-01) (the left diagram in Fig. 5A) [31,32], where hSYN of AAV2/9 is a neuron specific promoter

Fig. 4. Calcium influx induced in TRPV4^{+} neurons in culture. A. Fluorescence micrographs of neurons transducted with TRPV4-mCherry (red) shows significant Ca^{2+} influx through Ca^{2+} indicator (Fluo 4AM, green) under magnetic stimulation. B. In vitro Calcium imaging fluorescence fold change of TRPV4-His499-MNP-HisAb and TRPV4-His499-MNP in response to magnetic stimulation. n > 50 cells of three independent replicates were analyzed. C. In vitro Calcium imaging fluorescence fold change of TRPV4-His[499]-MNP-HisAb, ruthenium red (RR), and no magnet groups respectively, n > 50 cells of three independent replicates were analyzed.

Fig. 5. Magnetogenetic control of the mice rapid rotations around body axis. A. Picture illustrates the process of mice magnetic control of rotation behavior. B. Image of recording arena and trajectory of a representative TRPV4$^+$/MNP$^+$ mouse analyzed by Tracker software. Virus and MNPs were injected in the striatum. The mouse turned unilaterally around its body axis (only left turns) during 1 min magnetic stimulation (MS) (red line). Before MS (blue line) and after MS (green line) were indicated. C. Numbers of contralateral rotations of 12 trials (6 mice) were counted and analyzed by one-way ANOVA (p < 0.0001). D. Radius of the rotation of a representative TRPV4$^+$/MNP$^+$ mouse. E. Numbers of homolateral rotations of 12 trials (6 mice) were counted and analyzed by one-way ANOVA (p < 0.0001).
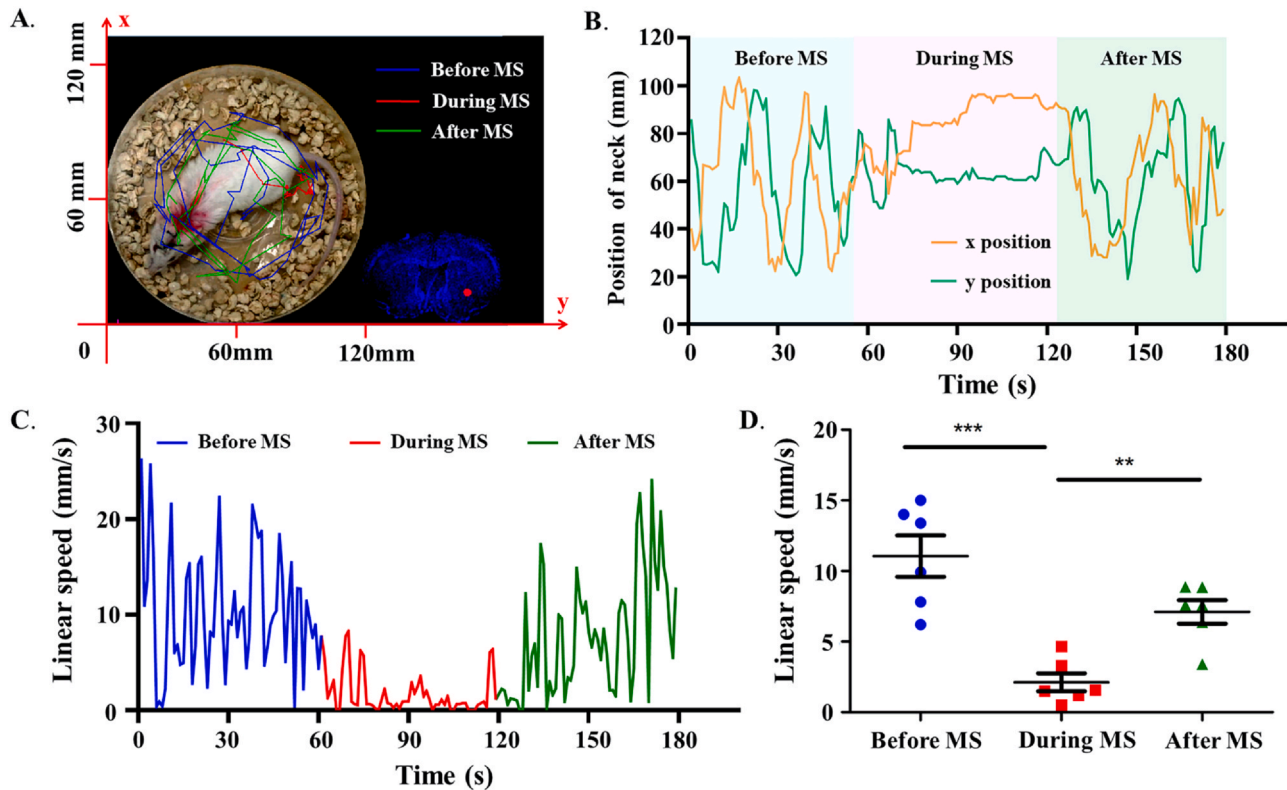
ensuring that TRPV4-His499 was only overexpressed in neurons. 600 nL Abs-modified MNPs were subsequently injected at the rate of 100 nL/min into the same position after 3 weeks(the middle diagram in Fig. 5A). The right diagram in Fig. 5A is the experimental set-up for *in vivo* magnetic stimulation (MS) in awake animals, mice were subjected to the magnetic field stimulation by putting a permanent magnet below them. It is worth noting that, to ensure the magnetic field sensed by animals changes dynamically within a certain range (about 200 mT), the mice were confined to a 3 cm high mobile arena, which keeps their heads in a horizontal position. The magnetic field produced by the permanent magnet was analyzed by K&J Magnetics (Fig. S10). The colocalization of MNPs and mCherry detected by immunofluorescence microscope was shown in Fig. S11. After adapting to the recording arena, the mice were stimulated and 3-minute videos were recorded for each trial including 1-min before-MS, 1-min during-MS and 1-min after-MS. Trajectory of a representative mouse was analyzed by Tracker (Fig. 5B, Movie S8). Red track line indicated the mouse made circles with smaller diameter which means the circles were rapid (with an average diameter of 35 ± 7 mm, Fig. 5B and D). Besides, we could tell from the videos

of 12 trials that the mice mainly turn left during the MS as the virus and MNPs were injected into the right part of the brain (Fig. 5B and C). Among the 12 trials, 10 trials showed totally 4–6 contralateral turns (left turn) during MS, and in 2 trials the mice turned right once, respectively (Fig. 5C and E). Control virus AAV-9-p2A-mCherry did not response to the MS with the existence of MNPs (Fig. S12, Movie S9).

Supplementary material related to this article can be found online at doi:10.1016/j.nantod.2021.101187.

Magnetic force drove deep brain stimulation at the deep striatum causes freezing of gait

To verify the validity of our magnetic nanotool in other behavior models, it was tested on the "freezing of gait" (FOG) behavior of mice. It is known that FOG is a common symptom in patients with advanced Parkinson disease, and optogenetic stimulation of the ridge between dorsal and ventral striatum caused FOG of mice [33,34]. The colocalization of MNPs and mCherry detected by immunofluorescence microscope was shown in Fig. S13. TRPV4-His^{499+}/

Fig. 6. Magnetogenetic control induced the mice freezing of gait (FOG). A. Image of recording arena and trajectory of a representative TRPV4-His^{499+}/MNP$^+$ mouse analyzed by Tracker software. Virus and MNPs were injected in the deep striatum (the ridge between dorsal and ventral striatum). Mouse track was recorded before MS (blue), during MS (red) and after MS (green) for 1 min, respectively. B. X and Y positions of mouse neck were analyzed. C. linear speed of the recorded mouse. D. Average linear speeds of 6 trials of 3 mice were analyzed before, during, and after the MS (one-way ANOVA, p < 0.001).

MNP$^+$ mice were observed to be able to move their heads but not the limbs during the MS. The movements were confined as shown by the red track of mouse and X and Y positions of neck (Fig. 6A and B, Movie S10). The linear speed of mouse was dramatically decreased to about 1.5 mm/s (Fig. 6C), and barely movement was detected. In our assay, 6 trials of 3 mice demonstrated consistent behaviors during their exposure to magnets, and with a significant low average linear speed compared with the absence of MS situation (Fig. 6D). Virus expression and MNPs binding were shown in Fig. 6A. Control virus AAV-9-p2A-mCherry did not response to the MS with the existence of MNPs (Fig. S14, Movie S11).

Supplementary material related to this article can be found online at doi:10.1016/j.nantod.2021.101187.

Therefore, the TRPV4-His^{499}-MNPs system is effective enough to evoke the calcium influx of neurons in vitro and activate neural system in vivo. TRPV4-based control of animal behaviors is solid and significant in our assay, indicating an effective non-invasive approach for modulation of neural system.

Discussion

This study raised the hypothesis of activating TRPV4 by MNPs based nanotool, and confirmed this neural stimulation method effective by realized the modulation of mice behavior by magnetic field. In this work, we used exogenous MNPs to open the TRPV4 ion channel. The colocation of His tag on TRPV4(TRPV4-His) and anti-His antibody modified MNPs are necessary in our magnetic sensitive tool.

For the TRPV4-His, the His tag inserted into the S1-S2 loop of TRPV4 seems much better than the other two designs. The probable explanation of this phenomenon is that His tag closer to the calcium ion channel (S5-S6) could affect the ions transit process in a way. For the MNPs used in this work, their properties were optimized to achieve successful genetic neurostimulation in vitro and in vivo. Firstly, the commercial MNPs has about cores with diameter of 20 nm, therefore, most of the MNPs are small enough (<30 nm) and enabled them to diffuse easily between the neurons in the brain [20]. Secondly, the superparamagnetic MNPs has been proven to be the preferred transducers for magnetic biostimulation [20], the MNPs used for the activation of TRPV4 were superparamagnetic and functionalized with carboxyl group which can improve hydrophilicity of MNPs and make the MNPs easier to immobilize proteins or antibodies [35,36]. Thirdly, in order to make the MNPs be targetable to specific cells or tissue sites and suitable for binding in mice brain, the MNPs used in this work were modified with anti-His antibody, which can also contribute to minimizing the amount of MNPs required for neurostimulation and reduce the negative effect of overheating in brain [35]. Additionally, during the calcium imaging assay, there was no increase in temperature of HEK293T cell culture media, which indicate that the MNPs used in this work didn't activate the temperature sensitive channel. Given the above, the commercial MNPs used in our assay have perfect magnetic responsiveness, and are suitable for the injection and binding in mice brain.

Neural modulation approaches including optogenetics, chemogenetics [37,38], sonogenetics [39,40], in which optogenetics has been successfully applied to the brain circuits' study of nonhuman primate [41], and has been developed and applied into the system neurosciences. Although optogenetics sheds light on the modulation of neural system and shows effective function on deep brain stimulation, non-invasive effective genetic based tools for the manipulating of neural activity still need to be explored and applied in future research. Magnetic force based nanotool as a newly emerged non-invasive approach, its development and application are growing into a hot area of research for the modulation of neural system.

Among the reported magnetic field based stimulation tool for neural control, they can mainly be divided into two types: single component tool made of TRPV-ferritin fusion protein, and double components tool composed of TRPV and magnetic nanoparticles. Both tools have been proved effective in the modulation of cell calcium transit or neural system [19–22]. TRPV1 and TRPV4 ion channels were targeted in these tools and assays were performed *in vitro* or *in vivo*. Our design is a double components tool in which MNPs play an important role in mechanical stimulating TRPV4 channel. Paramagnetic nanoparticles alone engaged in the regulation of neural system have been reported and confirmed to induce cortical neurons calcium influx in view of the 10–15% increase of the calcium fluorescent signal. N-type mechano-sensitive calcium ion channels were confirmed to be responsible for this process [42,43]. Although double components (two injections) are needed in this method based on TRPV4-His and anti-His antibody modified MNPs, negative effects related to off-target and overheating can be reduced in modulation of animal neural system.

To improve the ability of modulating neuronal activity, further research is required to make the MNPs have optimal performance. In addition to some basic parameters such as MNPs' size and magnetic properties, surface chemistry of MNPs plays a key role in their biological fate including cellular uptake, colloidal stability, toxicity, circulation, biodistribution and so on [35]. In future, various surface modification strategies need to be developed to reduce the noxious impact with neural tissues and improve the bioperformance of MNPs and the specificity of the functional outcome. Genetically magnetic control of neural system by MNPs is an effective way for avoid off-target effect, which is rapidly evolving but still at an early stage [44]. In the case of magnetothermal stimulation, the heating ability which related to the interaction between the size, microstructure and magnetic susceptibility of MNPs, should also be considered to avoid overheating or inefficient heat dissipation at the targeted region [45]. Although some MNPs have shown good biocompatibility, continued optimization and utilization of MNPs for neural stimulation are still needed, which exhibits great potential in better understanding neural function and clinical application.

Conclusion

Overall, we designed an effective non-invasive neural modulation nanotool composed of TRPV4 and MNPs under magnetic field stimulation, and successfully applied it into the control of freely moving mice behaviors. We explored this magnetic sensitive nanotool, and validated its use both *in vitro* and *in vivo* using calcium imaging and animal behavior control experiments. In mice, this nanotool was verified to elicit unilaterally rotation and "freezing of gait" behaviors. This work thus demonstrates a promising approach in the field of neural modulation, new circuits interpretation and disease treatment, and provides an useful validation study for magnetogenetics.

Experimental section

Animals

All animal procedures complied with the guidelines of the Recommendations from the Declaration of Helsinki, and were approved by the Institutional Animal Care and Use Committee of the Chinese Academy of Military Medical Science. We made all possible efforts to reduce the number of animals used. Pregnant Sprague–Dawley (SD) female rats and male BALB/c mice were bought from the Experimental Animal Center, Academy of Military Medical Science (Beijing, PRC). The rats and mice were placed in a room with constant temperature (24 ± 2 °C) and were housed in cages under a normal day/night cycle.

Molecular biology and virus packing

TRPV4-His[499], TRPV4-His[573], and TRPV4-His[688] DNA fragments were synthesized and cloned into pcDNA3.1 and pCDH-CMV-MCS-EF1-puro plasmids, respectively (General Biosystems, Inc.). pCDH-CMV-MCS-EF1-TRPV4-His[499]-P2A-mCherry plasmid was used for lenti-virus package together with the three package proteins(VSV, pMDlg, RSV-REV). AAV2/9-hSYN-TRPV4- His[499]-P2A-mCherrry-WPREs (1 × 10^{13} vg/ml) and AAV2/9-hSYN-P2A-mcherry-WPREs were used for neuronal cells transduction and obtained from BrainVTA Technology.

Magnets and magnetic field strength measurement

Electromagnets of varying sizes and strengths were purchased from XDA, China. Permanent N42- or N52-grade NdFeB magnets were purchased online (Taobao, M.PLAN). Gaussmeters (F.W.Bell, Inc.) was used to determine the field strength of electromagnets over distance for each experiment. For the *in vivo* mouse behavioral experiments using permanent NdFeB magnets, an online magnetic field calculator (K&J Magnetics) or a gaussmeter was used.

HEK293T cell culture and transfection

Cells used in this study were authenticated and checked for mycoplasma contamination. HEK293T cells were grown in Dulbecco's modified Eagle's media supplemented with 10% fetal bovine serum containing 1 × pen/strep (Invitrogen) and maintained at 37 °C in a humidified incubator with 5% CO2. Cells were transfected using Lipofectamine 3000 (Invitrogen) according to standard protocol provided by Invitrogen.

Neuron culture and transduction

Cortical tissues were dissected out from 17-day-old embryonic rats and were dissociated by enzymatic digestion in a 0.25% trypsin solution (30 min at 37 °C). The resulting tissue was resuspended in Dulbeccos modified Eagle's medium (DMEM, Sigma) containing 10% equine serum (Beyotime Biotechnology) and 5% fetal calf serum (Gibco) at a final concentration of 1×10^6 cells/ml. Cells were plated onto chamber slides previously coated with poly-L-lysine (Sigma, 0.1 mg/ml) and matrigel (Sigma, 0.2 mg/ml). After the cells were adhered onto the chamber slides, the medium was replaced by Neurobasal containing B-27, and half of the medium was changed every 2 days. All cells were placed in a humidified incubator (5% CO_2, 95% air, 37 °C). Cells were transducted using AAV according to standard protocol provided by BrainVTA.

Magnetic nanoparticle preparation and characterization

Commercial supermagnetic nanoparticles (MNPs) with a hydrodynamic diameter of about 100 nm were purchased from Chemicell, composed of magnetite core(20 ± 10 nm) and polysaccharide matrix, and functionalized with a glucuronic acid-carboxyl group. The MNPs were then coated with Anti-His tag antibody (Santa Cruz) using carbodiimide method, following the standard coupling procedure protocol provided by Chemicell(covalent coupling procedure on fluidMAG-ARA by carbodiimide method).

Labeling cells with MNPs

Culture media were removed and cells were washed 3 times with PBS. 10 μL MNPs in PBS (10 mg/ml) was added to cells and kept for 30 min incubation. Remove the unbounded MNPs with normal culture media or buffer.

Microscopy

Imaging for calcium imaging and immunocytochemistry was performed on a Nikon Ti-E Inverted Live Cell Imaging System. Calcium imaging was performed using 10 × magnification. Transmission electron microscope (Technai10, Philip, Eindhoven, The Netherlands) was used for the examination of MNPs. Confocal Laser microscope was used for cell fluorescence detection and brain slice scan (Nikon Ti-A1).

In vitro magnetic calcium imaging

Calcium imaging was performed according to the standard protocol provided by other lab [9]. Briefly, cells labeled with MNPs were washed three times with calcium imaging buffer (CIB) (105 mM NaCl, 3 mM KCl, 2.5 mM $CaCl_2$, 0.6 mM $MgCl_2$, 10 mM HEPES, 1.2 mM $NaHCO_3$, 100 mM mannitol and 10 mM glucose, adjusted to pH 7.45 with NaOH) and loaded with 3 μM Fluo-4AM diluted in CIB for 30 min at 37 °C. Cells were then washed three times with CIB and de-esterified for 30 min at 37 °C. Dishes were then loaded into customized imaging chambers and imaged at 10× magnification for analysis. Ruthenium red (RR), a TRP channel pore blocker (Sigma), was used at a work concentration of 10 nM and cells were incubated with RR for ~2–3 min in the imaging chambers before imaging. For calcium-free medium experiments, calcium in CIB was replaced with 10 mM EGTA and cells were washed and incubated with calcium-free medium. The TRPV4 specific antagonist GSK2193874 was purchased from Sigma and used at a work concentration of 10 nM. Cells were incubated in GSK2193874 for 5 min at 37 °C before calcium imaging. A magnetic stimulus was delivered using 3-cm electromagnet (rated for continuous duty, 12 V DC, 5 W and 10 kg of pull force). We situated the magnet directly above the imaging chamber during imaging. Using a gaussmeter, we calculated the magnetic field experienced by the cells (~0.5 cm away from the magnet) to be roughly 40–50 mT. Imaging was performed by recording 30 s of baseline fluorescence and then turning on the magnet for 3–6 pulses of 10 s each (0.1 Hz, total time of 30–60 s, 90% duty cycle), using a standard DC power delivery system. Cells were randomly selected from an image field. Quantification was performed by averaging 30 s of baseline fluorescence measurements with no applied magnetic field followed by quantification of the largest three fluorescence values following MS. The three peak values were normalized to the average baseline fluorescence before magnetic stimulation to compute a relative fold change for each cell. For time course analyses, fluorescence data for each cell were analyzed as a relative increase over time compared to the baseline fluorescence (30 s) before MS.

Evoking and observing animal behavior

Mice were anesthetized in an induction chamber (5% isoflurane) and placed in a stereotaxic frame (RWD Life Science) where they were maintained at 1–2% isoflurane throughout the procedure. A craniotomy was performed, and mice were injected with viruses or MNPs into different region. For dorsal striatum injections, 1 μL of AAV2/9-hSYN-TRPV4-His[499]-P2A-mCherrry-WPREs or control virus was injected at stereotaxic coordinates from bregma: 0 mm (AP), 2.3 mm (ml), and −3 mm (DV). For the ridge between dorsal and ventral striatum injections, 1 μL of AAV2/9-hSYN-TRPV4-His[499]-P2A-mCherrry-WPREs was injected at stereotaxic coordinates from bregma: 0,01 mm (AP), 2.3 mm (ml), and −4.1 mm (DV). Mice were allowed to recover for at least 3 weeks, allowing for optimal viral expression. Subsequently, 600 nL of MNPs (10 mg/ml) were injected into the same site as virus and mice behavior was detected the next day. Male BALB/c mice (3–4 week old, weighing 15–20 g) were used for the surgery.

Recording animal behavior

For each session, the animals were placed in a circular observation area. Sessions were limited to 10 min, including 3 min habituation, and 3–5 min experiment, during which about 200 mT magnetic stimulation was given. A consumer camera (Nikon D810) was used to record video (HD720, 60fps) of the mice before, during and after the magnetic field stimulation. Red marks were made on the mice with common marker pen (Sharpe) to aid motion tracking.

Behavioral analysis of freely moving mice

Motion tracking for all motor behavior analysis, the position of the red neck marker was recorded automatically using the free video analysis and modeling tool TRACKER built by Douglas Brown on the Open Source Physics Java framework. For the rotation motor response, every second frame was analyzed, resulting in 30 position measurements per second. The coordinates were produced by the Tracker to visualize the spatial motion XY-plots of the motion. For motion tracking of the 'freezing of gait' response, the position of each paw was tracked every 1 s and the speed of the mouse was calculated as the absolute value of the linear speed averaged over 3 s

Video editing for presentation

Videos chosen for publication were edited using Adobe Premiere software. Raw videos were compressed using H.264 encoder and down sampled to 24 fps and sped up 3X for fast download and observation. The red marks on the neck were applied to aid motion tracking. Field application periods and the MNPs injection sites in the brain are indicated in the video.

Histology

Frozen coronal Rostral to caudal brain sections were prepared following standard protocols. The 15 mm thick slices were stained with DAPI for subsequent laser confocal imaging.

Homology

Phyre2 (Protein Homology/analogY Recognition Engine) [46] was used to predict the three dimensional structures of the three His-tagged TRPV4 proteins.For each protein, the model with the highest rank was modeled based on XenopusTropicalis TRPV4 (Transient receptor potential cation channel, subfamily V, member 4, PDB ID: 6BBJ) with an identity percentage of 86%. The models were verified by checking the Rama chandran map and molecular dynamics (MD) simulations. The tetramers remained stable during MD simulations at 310 K and pH 7.0.

CRediT authorship contribution statement

S.W. and H.L. contributed equally to this work. C.W. and J.Z. supervised the project; S.W. and H.L. designed the project; S.W. carried out most of the experiments; D.W. carried out the homology modeling, D.W., L.Z. and Z.G. contributed to paper revising; X.Q., W.L. and Z.X. contributed to neural cell signaling recording and analysis; X.Q.,W.L., L.Z. and Z.X. contributed to figure arrangement and presentation. S.W. wrote the paper.

Declaration of Competing Interest

The authors declare that they have no known competing financial interests or personal relationships that could have appeared to influence the work reported in this paper.

Acknowledgements

Author contributions

W. and J.Z. supervised the project; S.W. and H.L. designed the project; S.W. carried out most of the experiments; D.W. carried out the homology modeling, D.W. and L.Z. contributed to paper revising; X.Q., W.L. and Z.X. contributed to neural cell signaling recording and analysis; X.Q.,W.L. and Z.X. contributed to figure arrangement and presentation. S.W. wrote the paper.

Appendix A. Supporting information

Supplementary data associated with this article can be found in the online version at doi:10.1016/j.nantod.2021.101187.

References

[1] X. Duan, T. Fu, J. Liu, C.M. Lieber, Nanoelectronics-biology frontier: from nanoscopic probes for action potential recording in live cells to three-dimensional cyborg tissues, Nano Today 8 (2013) 351–373.

[2] L. You, J. Wang, T. Liu, Y. Zhang, X. Han, T. Wang, S. Guo, T. Dong, J. Xu, G.J. Anderson, Q. Liu, Y. Chang, X. Lou, G. Nie, Targeted brain delivery of rabies virus glycoprotein 29-modified deferoxamine-loaded nanoparticles reverses functional deficits in parkinsonian mice, ACS Nano 12 (2018) 4123–4139.

[3] H.A. Ledesma, X. Li, J.L. Carvalhodesouza, W. Wei, F. Bezanilla, B. Tian, An atlas of nano-enabled neural interfaces, Nat. Nanotechnol. 14 (2019) 645–657.

[4] C. Nie, L. Ma, S. Li, X. Fan, Y. Yang, C. Cheng, W. Zhao, C. Zhao, Recent progresses in graphene based bio-functional nanostructures for advanced biological and cellular interfaces, Nano Today 26 (2019) 57–97.

[5] Y. Yang, Q. Wang, L. Song, X. Liu, P. Zhao, F. Zhang, N. Gu, J. Sun, Diverse functions and mechanisms of pericytes in ischemic stroke, Curr. Neuropharmacol. 15 (2017) 892–905.

[6] S. Ling, K. Jin, D.L. Kaplan, M.J. Buehler, Ultrathin free-standing bombyx mori silk nanofibril membranes, Nano Lett. 16 (2016) 3795–3800.

[7] H. Zhuang, S. Bu, L. Hua, M.A. Darabi, X. Cao, M. Xing, Gelatin-methacrylamide gel loaded with microspheres to deliver GDNF in bilayer collagen conduit promoting sciatic nerve growth, Int J. Nanomed. 11 (2016) 1383–1394.

[8] X. Xue, J. Yang, Y. He, L. Wang, P. Liu, L. Yu, G. Bi, M. Zhu, Y. Liu, R. Xiang, X. Yang, X. Fan, X. Wang, J. Qi, H. Zhang, T. Wei, W. Cui, G. Ge, Z. Xi, C. Wu, X. Liang, Aggregated single-walled carbon nanotubes attenuate the behavioural and neurochemical effects of methamphetamine in mice, Nat. Nanotechnol. 11 (2016) 613–620.

[9] F. Vitale, S.R. Summerson, B. Aazhang, C. Kemere, M. Pasquali, Neural stimulation and recording with bidirectional, soft carbon nanotube fiber microelectrodes, ACS Nano 9 (2015) 4465–4474.

[10] A. Galvan, M. Caiola, D.L. Albaugh, Advances in optogenetic and chemogenetic methods to study brain circuits in non-human primates, J. Neural Transm. (Vienna) 125 (2018) 547–563.

[11] A. Kumar, A. Tan, J. Wong, J.C. Spagnoli, J. Lam, B.D. Blevins, G. Natasha, L. Thorne, K. Ashkan, J. Xie, H. Liu, Nanotechnology for Neuroscience: Promising Approaches for Diagnostics, Therapeutics and Brain Activity Mapping, Adv. Funct. Mater. 27 (2017) 1700489.

[12] A. Marino, G.G. Genchi, V. Mattoli, G. Ciofani, Piezoelectric nanotransducers: The future of neural stimulation, Nano Today 14 (2017) 9–12.

[13] A. Marino, S. Arai, Y. Hou, E. Sinibaldi, M. Pellegrino, Y. Chang, B. Mazzolai, V. Mattoli, M. Suzuki, G. Ciofani, Piezoelectric Nanoparticle-Assisted Wireless Neuronal Stimulation, ACS Nano 9 (2015) 7678–7689.

[14] P. Rajasethupathy, E.A. Ferenczi, K. Deisseroth, Targeting Neural Circuits, Cell 165 (2016) 524–534.

[15] O. Yizhar, L.E. Fenno, T.J. Davidson, M. Mogri, K. Deisseroth, Optogenetics in neural systems, Neuron 71 (2011) 9–34.

[16] R. Chen, G. Romero, M. Christiansen, A. Mohr, P. Anikeeva, Wireless magnetothermal deep brain stimulation, Science 347 (2015) 1477–1480.

[17] S.H. Loukin, X. Zhou, Z. Su, Y. Saimi, C. Kung, Wild-type and brachyolmia-causing mutant TRPV4 channels respond directly to stretch force, J. Biol. Chem. 285 (2010) 27176–27181.

[18] M.A. Wheeler, C.J. Smith, M. Ottolini, B.S. Barker, A.M. Purohit, R.M. Grippo, R.P.A. Gaykema, A.J. Spano, M.P. Beenhakker, S. Kucenas, M.K. Patel, C.D. Deppmann, A.D. Guler, Genetically targeted magnetic control of the nervous system, Nat. Neurosci. 19 (2016) 756–761.

[19] S.A. Stanley, J.E. Gagner, S. Damanpour, M. Yoshida, J.S. Dordick, J.M. Friedman, Radio-wave heating of iron oxide nanoparticles can regulate plasma glucose in mice, Science 336 (2012) 604–608.

[20] R. Munshi, S. Qadri, Q. Zhang, I.C. Rubio, P.D. Pino, A. Pralle, Magnetothermal genetic deep brain stimulation of motor behaviors in awake, freely moving mice, Elife 6 (2017) e27069.

[21] S.A. Stanley, J. Sauer, R.S. Kane, J.S. Dordick, J.M. Friedman, Nat. Med. 21 (2015) 537–537.

[22] S.A. Stanley, L. Kelly, K.N. Latcha, S.F. Schmidt, X. Yu, A.R. Nectow, J. Sauer, J.P. Dyke, J.S. Dordick, J.M. Friedman, Bidirectional electromagnetic control of the hypothalamus regulates feeding and metabolism, Nature 531 (2016) 647–650.

[23] S. Nimpf, D.A. Keays, Is magnetogenetics the new optogenetics? EMBO J. 36 (2017) 1643–1646.

[24] M. Meister, Role of atomic spin-mechanical coupling in the problem of a magnetic biocompass, Phys. Rev. E 97 (2018) 042409.

[25] M.R. Loebinger, P.G. Kyrtatos, M. Turmaine, A.N. Price, Q.A. Pankhurst, M.F. Lythgoe, S.M. Janes, Magnetic resonance imaging of mesenchymal stem cells homing to pulmonary metastases using biocompatible magnetic nanoparticles, Cancer Res 69 (2009) 8862–8867.

[26] L.E. Gonzalezlara, X. Xu, K. Hofstetrova, A. Pniak, A. Brown, P.J. Foster, J. Neuro. Traum 26 (2009) 753–762.

[27] A. Cole, A.E. David, J. Wang, C.J. Galban, V.C. Yang, Magnetic brain tumor targeting and biodistribution of long-circulating PEG-modified, cross-linked starch-coated iron oxide nanoparticles, Biomaterials 32 (2011) 6291–6301.

[28] Z. Deng, N. Paknejad, G. Maksaev, M. Salarabanal, C.G. Nichols, R.K. Hite, P. Yuan, Cryo-EM and X-ray structures of TRPV4 reveal insight into ion permeation and gating mechanisms, Nat. Struct. Mol. Biol. 25 (2018) 252–260.

[29] A.C. Kreitzer, R.C. Malenka, Striatal plasticity and basal ganglia circuit function, Neuron 60 (2008) 543–554.

[30] B.R. Arenkiel, M.E. Klein, I.G. Davison, L.C. Katz, M.D. Ehlers, Genetic control of neuronal activity in mice conditionally expressing TRPV1, Nat. Methods 5 (2008) 299–302.

[31] N. Li, T. Chen, Z.V. Guo, C.R. Gerfen, K. Svoboda, A motor cortex circuit for motor planning and movement, Nature 519 (2015) 51–56.

[32] S.W. Oh, J.A. Harris, L. Ng, B. Winslow, N. Cain, S. Mihalas, Q. Wang, C. Lau, L. Kuan, A.M. Henry, M. Mortrud, B. Ouellette, T.N. Nguyen, S.A. Sorensen, C.R. Slaughterbeck, W. Wakeman, Y. Li, D. Feng, A. Ho, E. Nicholas, K.E. Hirokawa, P. Bohn, K.M. Joines, H. Peng, M. Hawrylycz, J.W. Phillips, J.G. Hohmann, P. Wohnoutka, C.R. Gerfen, C. Koch, A. Bernard, C. Dang, A.R. Jones, H. Zeng, A mesoscale connectome of the mouse brain, Nature 508 (2014) 207–214.

[33] A.V. Kravitz, B.S. Freeze, P.R.L. Parker, K. Kay, M.T. Thwin, K. Deisseroth, A.C. Kreitzer, Regulation of parkinsonian motor behaviours by optogenetic control of basal ganglia circuitry, Nature 466 (2010) 622–626.

[34] V. Gradinaru, M. Mogri, K.R. Thompson, J.M. Henderson, K. Deisseroth, Optical deconstruction of parkinsonian neural circuitry, Science 324 (2009) 354–359.

[35] I. Castellanos-Rubio, R. Munshi, S. Qadri, A. Pralle, Use Nanopart. Neurosci. NY (2018) 39–51.

[36] A. Akbarzadeh, M. Samiei, S. Davaran, Magnetic nanoparticles: preparation, physical properties, and applications in biomedicine, Nanoscale. Res. Lett. 7 (2012) 144.

[37] S.M. Sternson, B.L. Roth, Chemogenetic tools to interrogate brain functions, Annu. Rev. Neurosci. 37 (2014) 387–407.

[38] B.L. Roth, DREADDs for Neuroscientists, Neuron 89 (2016) 683–694.

[39] S. Ibsen, A. Tong, C. Schutt, S. Esener, S.H. Chalasani, Sonogenetics is a non-invasive approach to activating neurons in Caenorhabditis elegans, Nat. Commun. 6 (2015) 8264.

[40] J. Ye, S. Tang, L. Meng, X. Li, X. Wen, S. Chen, L. Niu, X. Li, W. Qiu, H. Hu, M. Jiang, S. Shang, Q. Shu, H. Zheng, S. Duan, Y. Li, Ultrasonic Control of Neural Activity through Activation of the Mechanosensitive Channel MscL, Nano Lett. 18 (2018) 4148–4155.

[41] K. Inoue, M. Takada, M. Matsumoto, Nat. Commun. 6 (2015) 8378-8378.

[42] A. Tay, A. Kunze, C. Murray, D.D. Carlo, Induction of Calcium Influx in Cortical Neural Networks by Nanomagnetic Forces, ACS Nano 10 (2016) 2331–2341.

[43] A. Tay, D.D. Carlo, Magnetic Nanoparticle-Based Mechanical Stimulation for Restoration of Mechano-Sensitive Ion Channel Equilibrium in Neural Networks, Nano Lett. 17 (2017) 886–892.

[44] E. Colombo, P. Feyen, M.R. Antognazza, G. Lanzani, F. Benfenati, Nanoparticles: A Challenging Vehicle for Neural Stimulation, Front. Neurosci. 10 (2016) 105.

[45] M. Colombo, S. Carregalromero, M.F. Casula, L. Gutierrez, M.D.P. Morales, I. Bohm, J.T. Heverhagen, D. Prosperi, W.J. Parak, Biological applications of magnetic nanoparticles, Chem. Soc. Rev. 41 (2012) 4306–4334.

[46] L.A. Kelley, S. Mezulis, C.M. Yates, M.N. Wass, M.J. Sternberg, The Phyre2 web portal for protein modeling, prediction and analysis, Nat. Protoc. 10 (2015) 845–858.